Research Article | Vol. 31, No. 2 / 16 Jan 2023 / Optics Express 1224
Optics EXPRESS

Wavefront recording plane-like method for polygon-based holograms

FAN WANG,[1,*] DAVID BLINDER,[2,3] TOMOYOSHI ITO,[1] AND TOMOYOSHI SHIMOBABA[1]

[1]Graduate School of Engineering, Chiba University, 1-33 Yayoi-cho, Inage-ku, Chiba, Chiba, Japan
[2]Department of Electronics and Informatics (ETRO), Vrije Universiteit Brussel (VUB), Pleinlaan 2, B-1050 Brussel, Belgium
[3]IMEC, Kapeldreef 75, B-3001 Leuven, Belgium
[*]wangfan@chiba-u.jp

Abstract: The wavefront recording plane (WRP) method is an algorithm for computer-generated holograms, which has significantly promoted the accelerated computation of point-based holograms. Similarly, in this paper, we propose a WRP-like method for polygon-based holograms. A WRP is placed near the object, and the diffracted fields of all polygons are aggregated in the WRP so that the fields propagating from the polygonal mesh affect only a small region of the plane rather than the full region. Unlike the conventional WRP method used in point-based holograms, the proposed WRP-like method utilizes sparse sampling in the frequency domain to significantly reduce the practical computational kernel size. The proposed WRP-like method and the analytical shading model are used to generate polygon-based holograms of multiple three-dimensional (3D) objects, which are then reproduced to confirm 3D perception. The results indicate that the proposed WRP-like method based on an analytical algorithm is hundreds of times faster than the reference full region sampling case; a hologram with tens of thousands of triangles can be computed in seconds even on a CPU, whereas previous methods required a graphics processing unit to achieve these speeds.

1. Introduction

An ideal three-dimensional (3D) display technology, like holography, must be able to record and reproduce the real wavefront emitted from an object so that it does not suffer from the vergence-accommodation conflict. Computer-generated holograms (CGHs) simulate the physical interference process of holography for non-existing 3D objects and can also be easily encoded onto spatial light modulators (SLMs) for electronic display [1]. Among the many 3D display technologies, CGHs are expected to provide high-quality dynamic 3D displays that can be used in next-generation interactive technologies, such as near-eye displays [2–4].

The massive computational effort required for CGH is one of the principal challenges for the implementation of CGHs to 3D displays. Many advanced algorithms have been proposed to simplify processes and accelerate computations [5,6], and to improve reconstruction quality [7,8]. Representative CGHs algorithms encompass layer-based [9,10], line-based [11,12], point-based [13,14] and polygon-based methods [15–17], real-valued holograms [18] and deep learning holograms [19,20]. Among them, point-based holograms are strongly developed by various acceleration algorithms, such as look-up tables (LUTs) [21] and wavefront recording planes (WRPs) [22]. By contrast, polygon-based holograms are still slightly inferior in computational efficiency.

Although, for polygon-based holograms, some improved analytical algorithms [23–26] save a large amount of overhead compared to numerical algorithms [15,27]; e.g., the LUTs method using principal component analysis has been proposed [28], and the controllable energy angular spectrum method (CE-ASM) reduces the computational effort by compacting the sampling

#479592 https://doi.org/10.1364/OE.479592
Journal © 2023 Received 2 Nov 2022; revised 13 Dec 2022; accepted 17 Dec 2022; published 3 Jan 2023

Optics EXPRESS

range in the frequency domain [29]. For polygon-based holograms, however, neither WRP techniques nor deep learning technologies have yet been proposed. Optical diffraction itself is a many-to-many process, so in the point-based holograms, the WRP is placed very close to the object point, which greatly reduces the coverage of the object point and thus reduces the computational effort [22,30]. However, since the polygon-based holograms address the angular spectrum of the object, the spectrum of the diffraction field will be spread over the entire frequency domain, which means that the point-based WRP is not applicable in polygon-based methods.

Matsushima *et al.* proposed region segmentation computation based on interpolation to reduce the computational area so that ultra-high resolution holograms can be computed with low memory [27,31]. In this paper, we follow this idea and propose a more general WRP-like method for analytical polygon-based holograms. Various methods are implemented on a CPU using MATLAB codes for comparison, and the results show that the proposed WRP-like method significantly improves computational efficiency. If parallel computation is performed on a graphics processing unit (GPU), the computation of polygon-based holograms will take a qualitative leap.

2. Principle: analytical algorithm for polygon-based holograms

An analytical polygon-based hologram can be calculated by an affine mapping with a fixed triangle, which offers an analytical spectral expression for all triangles. In the global coordinate system $Oxyz$, an arbitrary triangular mesh Γ with vertex coordinates $(x_i, y_i, z_i), i = \{1, 2, 3\}$, emits a plane light wave and propagates to the hologram plane ($z = 0$) along the z-axis, as shown in Fig. 1. Suppose that the transmittance of the mesh is uniform, the initial complex amplitude of the triangle Γ is given by:

$$E_0 = \exp(j2\pi z/\lambda), \tag{1}$$

where λ is the wavelength. From the angular spectrum diffraction, the spectrum of the triangle Γ in the hologram plane is

$$F = \iint_{\Gamma} E_0 \exp[-j2\pi(xf_x + yf_y + zf_z)]\mathrm{d}x\mathrm{d}y, \tag{2}$$

where $j = \sqrt{-1}$, $f_z = (\lambda^{-2} - f_x^2 - f_y^2)^{1/2}$, and f_x,f_y are sampling coordinates in frequency domain. The hologram is obtained by performing the inverse fast Fourier transform (iFFT) for the spectra F.

A fixed right triangle Δ with known vertices $(x_i', y_i', 0), i = \{1, 2, 3\}$ is located in the local coordinate system $O'x'y'z'$, where the origin is the triangle Γ's center of gravity and the w-axis is along the normal direction of the triangle Γ, as shown in Fig. 1. Based on the affine transformation, the triangle Γ can be represented by the triangle Δ through a matrix $\mathbf{T} = [T_{ij}]_{3\times4}$, where $\mathbf{T}$ can be addressed by the vertex coordinates of triangle Γ and Δ [28]; hence, Eq. (2) can be rewritten as:

$$F = J\exp(-j2\pi f_z') \iint_{\Delta} \exp[-j2\pi(x'f_x' + y'f_y')]\mathrm{d}x'\mathrm{d}y' = G(f_x', f_y', f_z') \tag{3}$$

where J is the Jacobian factor, $G(\cdot)$ denotes an analytical function of f_x',f_y' and f_z', which is given in Refs. [17,28]. The important variable (f_x', f_y', f_z') is the resampling of the regular grid (f_x, f_y) due to the affine transformation, determined by:

$$[f_x', f_y', 0, f_z'] = [f_x, f_y, f_z - 1/\lambda]\mathbf{T}. \tag{4}$$

Optics EXPRESS

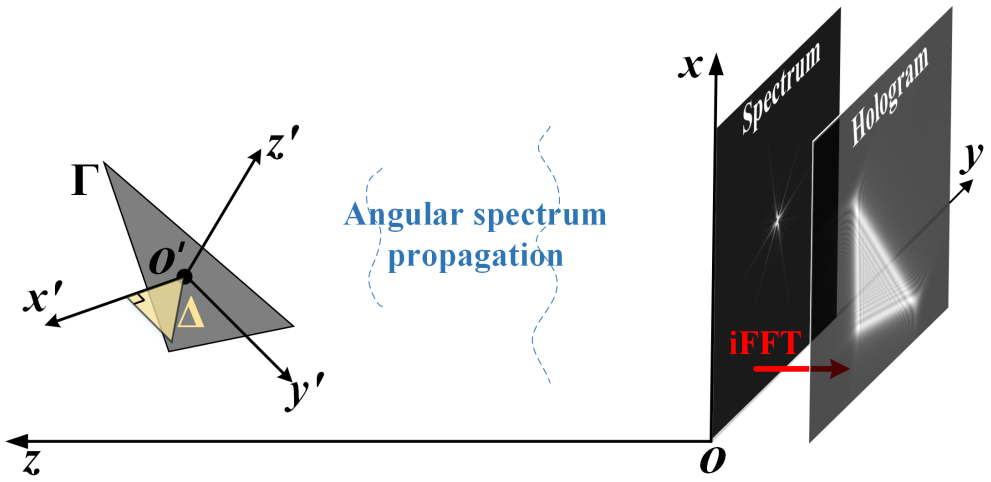

Fig. 1. Schematic of a polygon-based hologram. Triangle Γ in the global coordinate system $Oxyz$ and the fixed right triangle Δ in the local coordinate system $O'x'y'z'$ have a relationship of a 3D affine transformation.

3. Method: WRP-like for polygon-based holograms

In general, the spectrum of an arbitrary triangle is calculated by the analytical function $G(\cdot)$ under the regular sampling grid (f_x, f_y). As shown in Fig. 2(a), assuming that the hologram is sampled $N_x \times N_y$ pixels at p interval, its physical dimensions are $L_x = pN_x, L_y = pN_y$. In the frequency domain, f_x and f_y are defined as the grids:

$$\begin{cases} f_x(m) = -\frac{1}{2p} + m\delta_x, & m \in \{0, 1, \ldots, N_x - 1\} \\ f_y(n) = -\frac{1}{2p} + n\delta_y, & n \in \{0, 1, \ldots, N_y - 1\}, \end{cases} \tag{5}$$

where $\delta_x = 1/L_x, \delta_y = 1/L_y$ are the frequency sampling pitches. Substituting the above equation into Eqs. (3) and (4), the analytical function $G(\cdot)$ will be calculated for $N_x \times N_y$ pixels. Note that the sample count should be doubled if convolution errors are taken into account, otherwise it would lead to border artifacts, as demonstrated in Refs. [29,32]. To briefly illustrate the key idea of the proposed WRP-like method, we use the non-doubling case here.

The full region sampling given in Eq. (5) yields many redundant calculations, hence Fig. 2(b) shows a partial sampling of a region containing only triangles, which is sampled as $N_X \times N_Y$ at the same interval p. In the frequency domain, the regular sampling grids are

$$\begin{cases} f_X(m) = -\frac{1}{2p} + m\delta_X, & m \in \{0, 1, \ldots, N_X - 1\} \\ f_Y(n) = -\frac{1}{2p} + n\delta_Y, & n \in \{0, 1, \ldots, N_Y - 1\} \end{cases} \tag{6}$$

where $\delta_X = 1/(pN_X), \delta_Y = 1/(pN_Y)$ denote the new frequency sampling pitches. Figure 2 indicates that the new sampling coordinates (f_X, f_Y) shares the same spectral range $\left[-\frac{1}{2p}, \frac{1}{2p}\right)$ as the full-region sampling coordinates (f_x, f_y), but Eq. (6) is more sparsely spaced. The analytical function $G(\cdot)$ is required to calculate $N_X \times N_Y$ pixels, which is much less than the initial (f_x, f_y) given in Eq. (5). By performing an iFFT on the spectrum with sparse grids, a partial region that includes exactly the triangle can be obtained, which has the same pixel pitch as the hologram. This region is then superimposed on the corresponding position in the hologram sampling grid, as shown by the last step in Fig. 2(b).

Optics EXPRESS

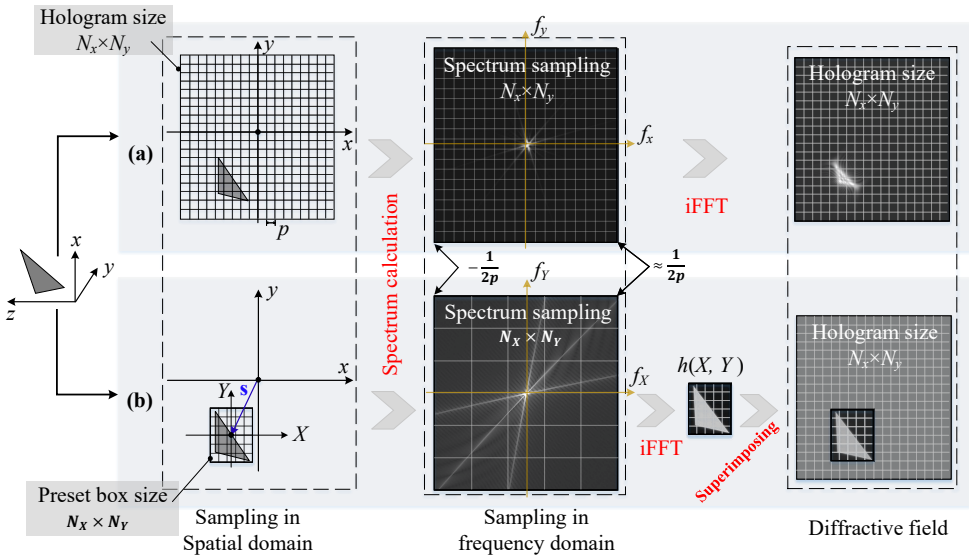

Fig. 2. (a) Sampling an arbitrary triangle with the full region of the hologram, calculating its spectrum with a dense frequency grid, and performing an iFFT on the spectrum to obtain diffracted field. (b) Sampling a partial region that contains exactly the triangle, calculating the spectrum with a sparse frequency grid, and performing an iFFT and superimposing it into the hologram sampling grid.

To receive the spectra of the triangles through the grid given in Eq. (6), we suggest a WRP which is very close to the triangles. As shown in Fig. (3)(a), like the point-based hologram, the WRP is parallel to the hologram plane, and the diffraction fields of the triangles or points are first recorded on the WRP. The diffraction at a close distance only affects small region rather than full region, which implies lighter calculations. Unlike the WRP of point clouds, recording a polygon-based hologram with WRP requires entering the frequency domain first and then returning to the spatial domain, as the process is shown in Fig. 2(b).

The preset area for recording triangles in the WRP depends on the diffraction angle, which is determined by the pixel pitch [33], defined as:

$$\theta = \sin^{-1}\left(\frac{\lambda}{2p}\right). \tag{7}$$

Assuming that the WRP is located at the Z plane, the preset area is given by:

$$\begin{cases} R = \max\limits_{i=1,2,3} (x_i + |z_i - Z| \cdot \tan\theta) \\ L = \min\limits_{i=1,2,3} (x_i - |z_i - Z| \cdot \tan\theta) \\ T = \max\limits_{i=1,2,3} (y_i + |z_i - Z| \cdot \tan\theta) \\ B = \min\limits_{i=1,2,3} (y_i - |z_i - Z| \cdot \tan\theta), \end{cases} \tag{8}$$

where R, L, T and B represent the right, left, top and bottom boundaries of the preset box, respectively, as shown in Fig. 3(b). The sampling number of this partial region defined in Fig. 2 can be solved by

$$N_X = \lceil (R - L)/p \rceil, \quad N_Y = \lceil (T - B)/p \rceil. \tag{9}$$

Optics EXPRESS

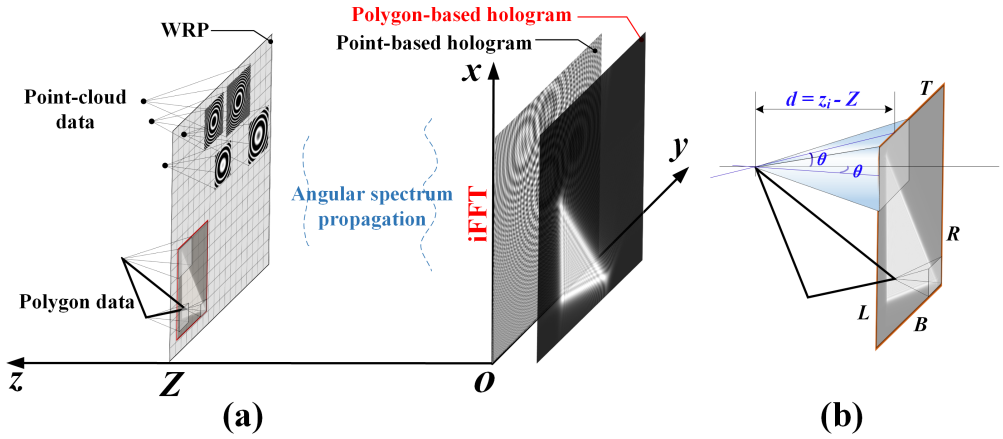

Fig. 3. (a) WRP method in a point-based hologram and the proposed WRP-like method in polygon-based hologram. WRP is placed close to the polygons or points, thus requiring only a small computational kernel. (b) Calculate the size of the preset box based on the diffraction angle and the vertex position.

Since the origin of the new sampling grid (f_x', f_y') does not match that of (f_x, f_y), a shifting factor must be taken into account here, given by a vector as follows:

$$\begin{aligned} \mathbf{s} &= [s_1, s_2] \\ &= [(R-L)/2, (T-B)/2], \end{aligned} \tag{10}$$

where s_1, s_2 are the components of $\mathbf{s}$. With the analytical equation given in Eq. (3), we can obtain the diffraction field of the triangle in the preset box, as follows:

$$h(X, Y) = \mathscr{F}^{-1}\{G(f_x', f_y', f_z') \cdot \exp[j2\pi(f_X s_1 + f_Y s_2]\}, \tag{11}$$

where (X, Y) is the sampling coordinate of the preset box in spatial domain, f_x', f_y' and f_z' are following to Eq. (4) based on the new sampling grid (f_X, f_Y) given in Eq. (6), and $\mathscr{F}^{-1}(\cdot)$ denotes the operator of iFFT.

For a 3D object consisting of N_t triangles, we can obtain $h_t(X, Y)$ for each triangle in its own preset area in the WRP according to Eqs. (8) to (11), so that the diffraction field of the whole object in the WRP can be expressed as:

$$h_{WRP}(x, y; z = Z) = \sum_{t=1}^{N_t} h_t(X, Y; x, y), \tag{12}$$

where $h_t(X, Y; x, y)$ represents that $h_t(X, Y)$ grid is superimposed into the corresponding hologram grid (x, y). Therefore, $h_{WRP}(x, y; z = Z)$ has been expanded to the same dimensions as the hologram, as shown in Fig. 2(b). As with the point-based WRP method, polygon-based holograms, $H(x, y)$, can be generated by propagating the angular spectrum of the WRP, as shown in Fig. 3(a), written as:

$$H(x, y) = \mathscr{F}^{-1}\left\{\mathscr{F}[h_{WRP}(x, y; Z)] \cdot \exp(-j2\pi f_z Z)\right\}, \tag{13}$$

where f_z is based on full region sampling grid determined by Eq. (5), and $\mathscr{F}(\cdot)$ denotes the operator of FFT.

Optics EXPRESS

4. Results

From the analysis of the full region sampling grid and partial region sampling grid in Section 3, only the region of interest needs to be calculated due to the setting of the WRP, which greatly reduces the computational load. Notably, since the full region sampling method is directly propagated to the hologram plane, the grid requires double sampling in the numerical calculation to avoid convolution errors, which further increases the workload. However, in the proposed WRP-like method, it extends the size of the preset box based on the diffraction angle and the distance from the triangle to the WRP given in Eqs. (7) and (8), which allows the calculation of the diffraction field in the WRP without double sampling, but only when the field of the WRP is diffracted toward the hologram plane, as Eq. (13).

To confirm the proposed WRP-like method for generating polygon-based holograms and its efficiency, we implemented different methods for 3D objects for comparison, as shown in Table 1 and Fig. 4. All holograms are sampled at 6.4μm interval with 1920 × 1080 pixels, and objects are diffracted to z = 10 mm. Table 1 shows the kernel sampling size in the practical calculation of each triangle, smaller computational kernel implies less workload. Due to double sampling to avoid convolution errors, full region sampling based on the analytical method calculates the largest kernel, which is four times the hologram sampling size [23,25,26]. The compact sampling based on the analytical method proposed in [29] saves about 30 times the kernel size compared to the full region sampling case, but further reduction affects the reproduction quality due to the loss of high frequencies. The application of the proposed WRP-like method to the polygon-based holograms can significantly reduce the size of the computational kernel, which relies on the size of triangular meshes. The more triangles that compose an object, the smaller the triangular mesh, which also implies the smaller the computational kernel of a single triangle. Table 1 shows the average kernel size of all triangles in the calculations of interpolation-based [27,31] and analytical-based WRP-like methods.

Table 1. The practical calculated kernel sample sizes for each triangle in computing holograms with 1920×1080 pixels.

Methods	Operators[a]	Number of triangles (N_t)						
		5,760	8,420	12,282	18,228	32,030	51,025	64,363
Full region sampling based on analytical method [23,25,26]	$G(\cdot)$: N_t iFFT : 1	3840×2160						
Compact sampling based on analytical method [29]	$G(\cdot)$: N_t iFFT : 1	342×1182						
Interpolation-based WRP-like method [31]	(i)FFT : $2N_t$+2 $\otimes$: $2N_t$	45×43[b]	28×30	70×70	11×15	18×18	25×26	20×21
Ours (Analytical-based WRP-like method)	$G(\cdot)$: N_t (i)FFT : N_t+2							

[a]Operation symbols and its number, where $G(\cdot)$ denotes the analytical function mentioned in Eq. (3) and $\otimes$ denotes the convolution operation. (i)FFT denotes including both FFT and iFFT operators.
[b]The computational kernel samples of the WRP-like method vary depending on the size of the triangular mesh, and the average size of all triangles is shown here.

Figure 4 shows the computational time of each method for each object. All holograms were generated in the MATLAB 2021a environment and the AMD Ryzen 5-3600 @3.59GH CPU. Since the GPU performs differently in different size of computational kernel, for a fair comparison, all calculations are performed in the CPU only. Since the proposed WRP-like method processes a very small computational kernel relative to compact sampling and full region sampling methods, the interpolation-based WRP-like method is about 20 times faster than the

Optics EXPRESS

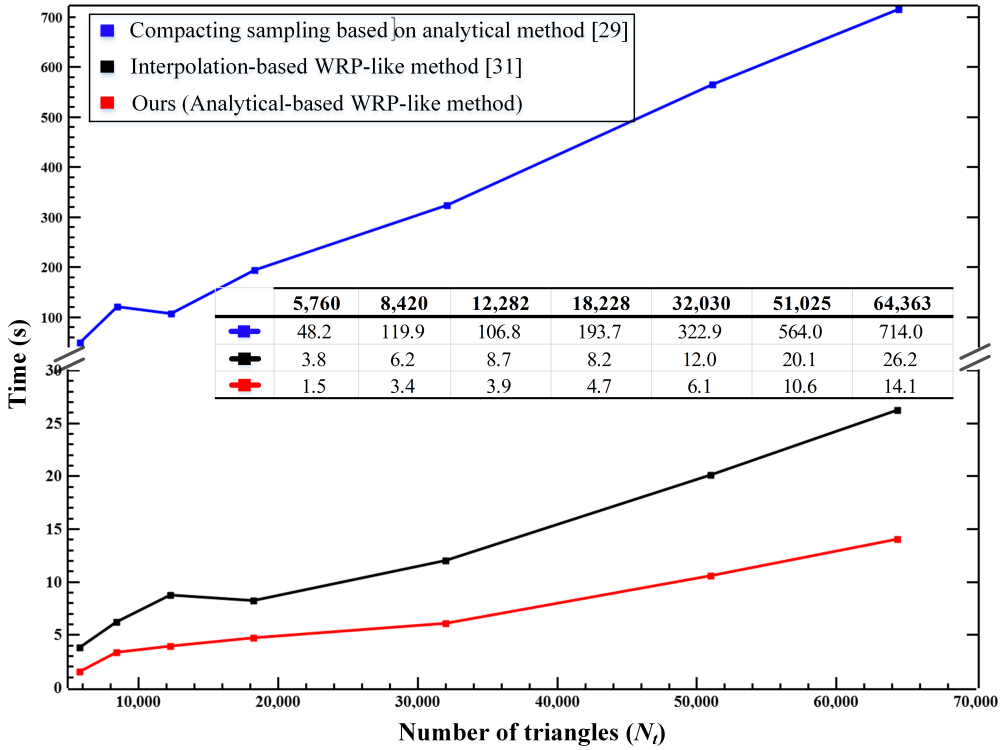

	5,760	8,420	12,282	18,228	32,030	51,025	64,363
	48.2	119.9	106.8	193.7	322.9	564.0	714.0
	3.8	6.2	8.7	8.2	12.0	20.1	26.2
	1.5	3.4	3.9	4.7	6.1	10.6	14.1

Fig. 4. The computational time on the CPU for each method for the hologram with 1920×1080 pixels. The table inside lists the detailed time (in seconds) calculated for each object corresponding to the Table 1. The results of the full region sampling based on the analytical method are not shown here because it is too time-consuming.

compact sampling based on the analytical function. The smaller the triangular mesh implies the smaller the computational kernel, which allows for faster acceleration. Due to the absence of interpolation and fewer FFT operations, the analytical-based WRP-like method is faster than the interpolation-based WRP-like method by a factor of more than two. The efficiency of the full region sampling based on the analytical method is not shown in Fig. 4 because it is too time-consuming. Figure 4 proves that the proposed WRP-like method can be widely used in the calculation of polygon-based holograms and also shows outstanding performance in terms of computational efficiency.

To reflect the 3D perception of the hologram, a bee composed of 51731 triangles, as shown in Fig. 5(a), is used to generate a hologram with 1024×1024 pixels using the proposed WRP-like method, as shown in Fig. 5(b). Figures 5(c) and 5(d) show the digital reconstructions of simulation at different distances. The depth of the bee is -2 mm to 2 mm. The hologram is in the $z = 0$ mm plane, where the WRP is also located and is rendered by our shading method [17]. Figure 5(c) reconstructed at -1.2 mm, which focuses on the right hind foot of the bee; Fig. 5(d) reconstructed at 1.5 mm, which focuses on the right wing of the bee. A set of dynamic holograms was generated by capturing the multiple motion states of the bee, and reconstructed at the same position (the right antenna of a bee), as shown in Visualization 1. The varifocal reconstruction is shown in Visualization 2.

Optics EXPRESS

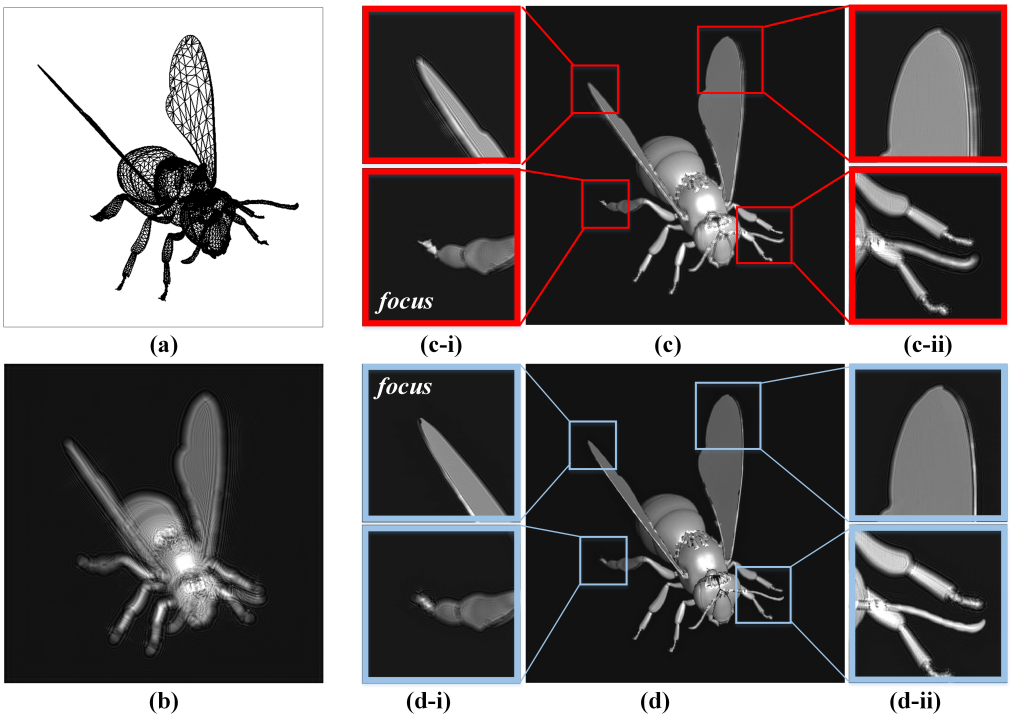

Fig. 5. (a) The 3D model of the bee with 51731 triangles and the remaining 24640 triangles after back-face culling. (b) The hologram generated by the proposed WRP-like method combined with the analytical shading method [17]. (c) Numerical reconstruction at the −1.2 mm, focusing on the right hind foot. (d) Numerical reconstruction at the 1.5 mm, focusing on the right wing. (c-i), (c-ii) and (d-i), (d-ii) are the enlarged portion of the box in (c) and (d), respectively.

5. Conclusion

In this manuscript, a WRP-like method for generating polygon-based holograms was proposed. Similarly to the WRP method in the point-based algorithm [22,30], the proposed method places a plane with the same dimension as the hologram near the object. The triangles were first diffracted into this plane and were recorded in a small partial region according to the diffraction angle. The sample size of the partial region rather than the full region was used as the practical computational kernel, which offers the potential for accelerating computation. Unlike the WRP method in the point-based algorithm, the proposed WRP-like method in the polygon-based algorithm requires first access to the frequency domain, where sparse frequency sampling is used to obtain the spectrum, and then returns to the spatial domain. The angular spectrum propagation of the WRP is the same as that of the point-based WRP method.

The proposed WRP-like method in polygon-based hologram is confirmed by calculations on several 3D objects. The computational results in the CPU indicate that the WRP-like method applied to the analytical-based algorithm is 50 times faster than the previously proposed compact-sampling method [29], and hundreds of times faster than the full region sampling method [23,25,26]. This is an exciting boost for polygon-based holograms.

Funding. Fonds Wetenschappelijk Onderzoek (12ZQ220N, 12ZQ223N, VS07820N); Japan Society for the Promotion of Science (19H01097, 22H03607).

Optics EXPRESS

Acknowledgements. We thank the Ministry of Education, Culture, Sports, Science and Technology (MEXT) of Japan and the China Scholarship Council (CSC) for their support.

Disclosures. The authors declare no conflicts of interest.

Data Availability. Data underlying the results presented in this paper are not publicly available at this time but may be obtained from the authors upon reasonable request.

References

1. T. Shimobaba and T. Ito, *Computer Holography: Acceleration Algorithms and Hardware Implementations* (CRC press, 2019).
2. D. Blinder, T. Birnbaum, T. Ito, and T. Shimobaba, "The state-of-the-art in computer generated holography for 3d display," Light: Adv. Manufact. **3**(3), 1–29 (2022).
3. C. Chang, K. Bang, G. Wetzstein, B. Lee, and L. Gao, "Toward the next-generation vr/ar optics: a review of holographic near-eye displays from a human-centric perspective," Optica **7**(11), 1563–1578 (2020).
4. Z. He, X. Sui, G. Jin, and L. Cao, "Progress in virtual reality and augmented reality based on holographic display," Appl. Opt. **58**(5), A74–A81 (2019).
5. E. Sahin, E. Stoykova, J. Mäkinen, and A. Gotchev, "Computer-generated holograms for 3d imaging: a survey," ACM Comput. Surv. **53**(2), 1–35 (2021).
6. D. Pi, J. Liu, and Y. Wang, "Review of computer-generated hologram algorithms for color dynamic holographic three-dimensional display," Light: Sci. Appl. **11**(1), 231 (2022).
7. M. Gopakumar, J. Kim, S. Choi, Y. Peng, and G. Wetzstein, "Unfiltered holography: optimizing high diffraction orders without optical filtering for compact holographic displays," Opt. Lett. **46**(23), 5822–5825 (2021).
8. X. Sui, Z. He, G. Jin, and L. Cao, "Spectral-envelope modulated double-phase method for computer-generated holography," Opt. Express **30**(17), 30552–30563 (2022).
9. Y. Zhao, L. Cao, H. Zhang, D. Kong, and G. Jin, "Accurate calculation of computer-generated holograms using angular-spectrum layer-oriented method," Opt. Express **23**(20), 25440–25449 (2015).
10. J. Jia, J. Si, and D. Chu, "Fast two-step layer-based method for computer generated hologram using sub-sparse 2d fast fourier transform," Opt. Express **26**(13), 17487–17497 (2018).
11. D. Blinder, T. Nishitsuji, and P. Schelkens, "Real-time computation of 3d wireframes in computer-generated holography," IEEE Trans. on Image Process. **30**, 9418–9428 (2021).
12. T. Nishitsuji, T. Shimobaba, T. Kakue, and T. Ito, "Fast calculation of computer-generated hologram of line-drawn objects without fft," Opt. Express **28**(11), 15907–15924 (2020).
13. P. Tsang, T.-C. Poon, and Y. Wu, "Review of fast methods for point-based computer-generated holography," Photonics Res. **6**(9), 837–846 (2018).
14. Y. Yamamoto, H. Nakayama, N. Takada, T. Nishitsuji, T. Sugie, T. Kakue, T. Shimobaba, and T. Ito, "Large-scale electroholography by horn-8 from a point-cloud model with 400, 000 points," Opt. Express **26**(26), 34259–34265 (2018).
15. K. Matsushima, "Computer-generated holograms for three-dimensional surface objects with shade and texture," Appl. Opt. **44**(22), 4607–4614 (2005).
16. Y. Zhang, H. Fan, F. Wang, X. Gu, X. Qian, and T.-C. Poon, "Polygon-based computer-generated holography: a review of fundamentals and recent progress," Appl. Opt. **61**(5), B363–B374 (2022).
17. F. Wang, H. Shiomi, T. Ito, T. Kakue, and T. Shimobaba, "Fully analytic shading model with specular reflections for polygon-based hologram," Opt. Lasers Eng. **160**, 107235 (2023).
18. T. Shimobaba, T. Tahara, I. Hoshi, H. Shiomi, F. Wang, T. Hara, T. Kakue, and T. Ito, "Real-valued diffraction calculations for computational holography," Appl. Opt. **61**(5), B96–B102 (2022).
19. L. Shi, B. Li, and W. Matusik, "End-to-end learning of 3d phase-only holograms for holographic display," Light: Sci. Appl. **11**(1), 247 (2022).
20. Y. Peng, S. Choi, N. Padmanaban, and G. Wetzstein, "Neural holography with camera-in-the-loop training," ACM Trans. Graph. **39**(6), 1–14 (2020).
21. Y. Pan, X. Xu, S. Solanki, X. Liang, R. B. A. Tanjung, C. Tan, and T.-C. Chong, "Fast cgh computation using s-lut on gpu," Opt. Express **17**(21), 18543–18555 (2009).
22. T. Shimobaba, N. Masuda, and T. Ito, "Simple and fast calculation algorithm for computer-generated hologram with wavefront recording plane," Opt. Lett. **34**(20), 3133–3135 (2009).
23. Y. Pan, Y. Wang, J. Liu, X. Li, and J. Jia, "Improved full analytical polygon-based method using fourier analysis of the three-dimensional affine transformation," Appl. Opt. **53**(7), 1354–1362 (2014).
24. D. Im, J. Cho, J. Hahn, B. Lee, and H. Kim, "Accelerated synthesis algorithm of polygon computer-generated holograms," Opt. Express **23**(3), 2863–2871 (2015).
25. Y.-P. Zhang, F. Wang, T.-C. Poon, S. Fan, and W. Xu, "Fast generation of full analytical polygon-based computer-generated holograms," Opt. Express **26**(15), 19206–19224 (2018).
26. H. Fan, B. Zhang, Y. Zhang, F. Wang, W. Qin, Q. Fu, and T.-C. Poon, "Fast 3d analytical affine transformation for polygon-based computer-generated holograms," Appl. Sci. **12**(14), 6873 (2022).
27. K. Matsushima and S. Nakahara, "Extremely high-definition full-parallax computer-generated hologram created by the polygon-based method," Appl. Opt. **48**(34), H54–H63 (2009).

Optics EXPRESS

28. F. Wang, T. Shimobaba, Y. Zhang, T. Kakue, and T. Ito, "Acceleration of polygon-based computer-generated holograms using look-up tables and reduction of the table size via principal component analysis," Opt. Express **29**(22), 35442–35455 (2021).
29. F. Wang, T. Shimobaba, T. Kakue, and T. Ito, "Controllable energy angular spectrum method," Opt. Commun. **520**, 128506 (2022).
30. P. Tsang and T.-C. Poon, "Review on theory and applications of wavefront recording plane framework in generation and processing of digital holograms," Chin. Opt. Lett. **11**(1), 010902 (2013).
31. K. Matsushima and S. Nakahara, "Region segmentation and parallel processing for creating large-scale cghs in polygon source method," in *Practical Holography XXIII: Materials and Applications*, vol. 7233 (SPIE, 2009), pp. 104–111.
32. K. Matsushima and T. Shimobaba, "Band-limited angular spectrum method for numerical simulation of free-space propagation in far and near fields," Opt. Express **17**(22), 19662–19673 (2009).
33. T.-C. Poon and J.-P. Liu, *Introduction to modern digital holography: with MATLAB* (Cambridge University Press, 2014).